Modified Tinkham's Equation for Exact Computation of a Thin Film Terahertz Complex Conductivity

Maxim S. Meged[1] · Anton D. Zaitsev[1,2] · Petr S. Demchenko[1,2,3] ·
Mikhail K. Khodzitsky[2,3]

Abstract

The progress in the development of THz (terahertz) photonics is associated with the application of new materials, including thin films with material parameters differing noticeably from these of bulk media or being difficult to predict by using various models. As a rule, the conductivity of a thin film placed on a dielectric substrate is investigated using an equation proposed by M. Tinkham in 1956. This equation does not take into account internal reflections and losses in a substrate; therefore, a filtering of THz waveforms is also required. In this work, we propose a modified equation which does not require preliminary waveform filtering and accounts for losses and internal reflections inside a substrate. Thus, it does not distort an information on material parameters of a thin-film sample. The derived method allows one to obtain an exact complex conductivity/permittivity dispersion of a thin film, which is confirmed by calculations based on the transfer matrix method and Drude-Smith model.

✉ Anton D. Zaitsev
  a.zaytsev@niuitmo.ru

  Maxim S. Meged
  rem3095@yandex.ru

  Petr S. Demchenko
  petr.s.demchenko@gmail.com

  Mikhail K. Khodzitsky
  khodzitskiy@yandex.ru

1 ITMO University, 49-A Kronverksky St., St. Petersburg 197101, Russia

2 Terahertz Photonics LLC, 180/2-A Nevskiy Ave., St. Petersburg 191167, Russia

3 Tydex LLC, 16 Domostroitelnaya St., St. Petersburg 194292, Russia

1 Introduction

The field of terahertz (THz) photonics is being intensively developed at the present time due to possibilities opened in last few decades only with a development of efficient and affordable emitters and detectors of THz radiation [1–3]. It is already being used in next-generation wireless communications, contactless diagnostics and imaging in medicine, security systems, pharmaceutics, food industry, etc. [4–6]

The progress in the development of THz technologies is associated with the application of new materials, including thin conductive films with material parameters (e.g., complex permittivity/conductivity) differing noticeably from these of bulk media or being difficult to predict by using various models [7]. As a rule, thin film is placed on a dielectric substrate transparent for THz waves. Complex amplitude spectra are measured for THz pulses transmitted through an air, a bare substrate, and a film-on-substrate structure by means of a terahertz time-domain spectroscopy (THz TDS) [8]. Then, thin film conductance is calculated using an equation proposed by M. Tinkham in 1956 [9]. However, this equation does not take into account the imaginary part of a substrate refractive index and internal reflections in it; therefore, a separate filtering of THz waveforms is also required.

In this work, we introduce a modified equation which does not require preliminary waveform filtering and accounts for losses and internal reflections inside a substrate. It allows one to obtain an exact complex conductivity/permittivity dispersion of a thin film, which is confirmed by calculations based on the transfer matrix method (TMM) [10] and Drude-Smith model for conductive materials [11]. As materials under study, thin bismuth film and single-layer graphene were chosen since they are often used in THz photonics [12, 13].

2 Methods

2.1 THz TDS

The simplified sketch of a THz TDS setup is presented in Fig. 1a. An initial 1560 nm femtosecond (fs) laser pulse is split into pumping and probing pulses by a polarization beam-splitter. The pumping pulse reaches a photoconductive switch, which produces a THz pulse subsequently passing through a sample object. The probing pulse passes through a tunable optical delay line. Both signals reach a detector (photoconductive switch). A recorded current is proportional to an amplitude of the THz pulse electric field at the moment of arrival of the probing fs pulse (THz field varies slowly compared to a duration of fs pulse). Thus, by changing a time delay of the pulses relative to each other using the optical delay line, the THz pulse waveform is recorded. To perform these measurements, the spectrometer TERA K15 by Menlo Systems with a spectral range of 2 THz, maximum dynamic range of 65 dB, and a maximum frequency resolution less than 1.2 GHz was used.

Figure 1b illustrates optical paths of three signals measured using THz TDS that pass through an air, a substrate, and a film-on-substrate medium. The problem being resolved in this work is related mainly to internal reflections inside the substrate.
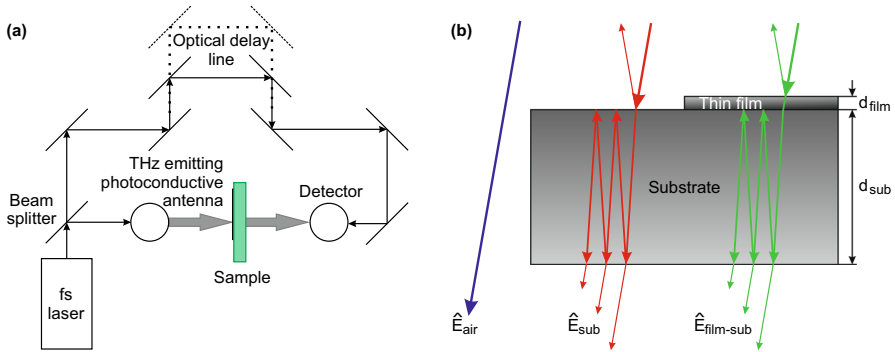
Fig. 1 **a** Simplified scheme of a THz TDS setup. **b** Sketch of a film-on-substrate sample and optical paths of three measured signals (the rays are depicted at an angle for clarity, while for the derivation, the normal incidence is assumed)

It should be mentioned that instead of THz TDS, VNA with extender and sub-harmonic mixer may be applied in order to measure complex amplitude spectra used in further calculations [14]. However, unlike THz TDS, this method allows one to perform spectroscopic measurements in a narrow frequency range depending on extender parameters.

2.2 Material Parameters Extraction

To measure a thin film conductivity dispersion, three time-dependent waveforms are recorded for a THz wave transmitted through an air (reference signal), a bare substrate, and a film-on-substrate structure. Then, they are converted into corresponding complex amplitude spectra ($\hat{E} = |\hat{E}|e^{i\phi}$) consisting of magnitudes $|\hat{E}(f)|$ and phases $\phi(f)$. Substrate complex refractive index dispersion is approximately defined as [15, 16]

$$n'_{sub}(f) = \frac{c\left[\phi_{sub}(f) - \phi_{air}(f)\right]}{2\pi f d_{sub}} + n_{air}, \tag{1a}$$

$$T_{sub}(f) = \frac{4n'_{sub}(f)n_{air}}{[n'_{sub}(f) + n_{air}]^2}, \tag{1b}$$

$$n''_{sub}(f) = \frac{c\ln\left[T_{sub}(f)/|\hat{E}_{sub}(f)/\hat{E}_{air}(f)|\right]}{2\pi f d_{sub}}, \tag{1c}$$

$$\hat{n}_{sub}(f) = n'_{sub}(f) - in''_{sub}(f), \tag{1d}$$

where c is the speed of light in vacuum, n_{air} is the air refractive index, f is a THz radiation frequency, $\hat{E}_{sub}(f)$ and $\hat{E}_{air}(f)$ are complex amplitude spectra of a THz wave passed through a substrate and an air correspondingly, $\phi_{sub}(f)$ and $\phi_{air}(f)$ are corresponding phases, d_{sub} is a substrate thickness, $T_{sub}(f)$ is a Fresnel power transmission coefficient, and i represents the imaginary unit. Equation 1 may give an error for absorbing substrate since it does not take into account the mutual influence of

real and imaginary parts of $\hat{n}_{sub}(f)$ on each other. To get an exact value of $\hat{n}_{sub}(f)$, an iterative method that takes into account a complex transmission coefficient is applied [16, 17]. Briefly, the initial value of the complex refractive index (extracted through Eq. 1) is used to calculate complex transfer function as

$$\hat{H}_{model}(f) = \frac{4\hat{n}_{sub}(f)n_{air}}{\left[\hat{n}_{sub}(f) + n_{air}\right]^2} \cdot exp\left(-i\left[\hat{n}_{sub}(f) - n_{air}\right]\frac{2\pi f d_{sub}}{c}\right) \cdot \hat{FP}(f),$$

(2)

where the first term is a complex transmission coefficient, and the last one is responsible for multiple reflections inside the substrate (Fabry-Pérot effect):

$$\hat{FP}(f) = \left(1 - \left[\frac{\hat{n}_{sub}(f) - n_{air}}{\hat{n}_{sub}(f) + n_{air}}\right]^2 \cdot exp\left[-2i\hat{n}_{sub}(f)\frac{2\pi f d_{sub}}{c}\right]\right)^{-1}. \quad (3)$$

This transfer function is compared with that measured in an experiment ($\hat{H}_{measured}(f) = \hat{E}_{medium}(f)/\hat{E}_{air}(f)$), after which the error is calculated and corresponding correction is taken in values of real and imaginary parts of a complex refractive index:

$$ER_m(f) = |\hat{H}_{measured}(f)| - |\hat{H}_{model}(f)|, \quad (4a)$$
$$ER_p(f) = \angle\hat{H}_{measured}(f) - \angle\hat{H}_{model}(f), \quad (4b)$$

$$Re[\hat{n}_{sub,new}(f)] = Re[\hat{n}_{sub,old}(f)] - s \cdot ER_p(f), \quad (5a)$$
$$Im[\hat{n}_{sub,new}(f)] = Im[\hat{n}_{sub,old}(f)] - s \cdot ER_m(f), \quad (5b)$$

where $ER_m(f)$ and $ER_p(f)$ are frequency-dependent magnitude and phase errors, $\hat{n}_{sub,new}(f)$ and $\hat{n}_{sub,old}(f)$ are substrate complex refractive index dispersions at current and previous stages of the algorithm, and s is the correction factor, typically set to 0.01 to ensure the algorithm convergence. The procedure is repeated until a difference between measured and calculated transfer functions is less than a specified error.

2.3 Tinkham's Equation

According to Tinkham's method [9], conductance dispersion of a thin film placed on a dielectric substrate is extracted as

$$\hat{\sigma}_{film}(f) = \frac{\hat{n}_{sub}(f) + 1}{Z_0}\left[\frac{\hat{E}_{sub}(f)}{\hat{E}_{film+sub}(f)} - 1\right], \quad (6)$$

where $\hat{E}_{film+sub}(f)$ is a complex amplitude spectrum of a wave passed through a film-on-substrate medium, and $Z_0 = 376.7$ Ohms is the free space impedance. If an

exact thickness of a thin film d_{film} is known, this conductance dispersion may be converted into permittivity dispersion of a film as [18]

$$\hat{\varepsilon}_{film}(f) = 1 + i\hat{\sigma}_{film}(f)/(2\pi f d_{film}\varepsilon_0), \tag{7}$$

where $\varepsilon_0 = 8.854 \cdot 10^{-12}$ F·m^{-1} is the absolute vacuum dielectric constant.

The disadvantage of Eq. 6 is neglecting internal reflections inside the plane-parallel substrate. More accurate approach, requiring filtering of waveforms, was presented in a work by Yan et al. [8]. Its idea is to get a conductivity separately from a first impulse and a first inner-reflected signal and then to predict a surface conductivity using both observations.

2.4 Modified Equation

A thin film is treated as a source of surface conductivity $\hat{\sigma}_{film}$ only on a fringe between a substrate and air. As a result, regardless of an incident light polarization, complex amplitude transmission and reflection coefficients are written as follows [19]:

$$\hat{t}_{1,2} = \frac{2\hat{n}_1}{\hat{n}_1 + \hat{n}_2 + Z_0\hat{\sigma}_{film}}, \tag{8a}$$

$$\hat{r}_{1,2} = \frac{\hat{n}_1 - \hat{n}_2 - Z_0\hat{\sigma}_{film}}{\hat{n}_1 + \hat{n}_2 + Z_0\hat{\sigma}_{film}}, \tag{8b}$$

where $\hat{t}_{1,2}$ and $\hat{r}_{1,2}$ denote complex amplitude transmission and reflection coefficients of a radiation propagating from a medium "1" to medium "2," and $\hat{n}_1$ and $\hat{n}_2$ are complex refractive indices of these media correspondingly.

Using these amplitude coefficients and following the optical paths of transmitted and reflected signals depicted in Fig. 1b, one may obtain complex amplitude transmission $\hat{t}$ and reflection $\hat{r}$ coefficients of an effective film-on-substrate medium taking into account internal reflections of a signal inside a substrate, denoted by $\hat{FP}$ term in equations below:

$$\hat{t} = \frac{\hat{E}_{film+sub}}{\hat{E}_{air}} = \hat{t}_{air,film}\hat{t}_{film,sub}\hat{t}_{sub,air}e^{i\hat{\delta}}\hat{FP}, \tag{9a}$$

$$\hat{r} = \hat{r}_{air,film} + \hat{t}_{air,film}\hat{r}_{sub,air}\hat{t}_{film,air}e^{i\hat{\delta}}\hat{FP}, \tag{9b}$$

$$\hat{FP} = \sum_{m=1}^{\infty}(\hat{r}_{sub,air}\hat{r}_{film,air}e^{i\hat{\delta}})^m = [1 - \hat{r}_{sub,air}\hat{r}_{film,air}e^{i\hat{\delta}}]^{-1}, \tag{9c}$$

where $\hat{\delta}(f) = 4\pi f d_{sub}\hat{n}_{sub}(f)/c$ is the term related to phase delay and extinction of a wave reflected twice in a substrate, and the complex refractive index is written as $\hat{n}_{sub}(f) = n'_{sub}(f) - in''_{sub}(f)$. The transmission between a film and a substrate is considered to be $\hat{t}_{film,sub} = 1$.

These equations may be solved numerically [20], but a mathematical derivation of the complex conductance $\hat{\sigma}_{film}$ is possible without simplifications. Depending on present experimental spectra, the following equations for a sheet conductance may be determined from transmittance measurements:

$$\hat{\sigma}_{film} = \frac{1}{Z_0} \frac{(\hat{n}_{sub}+1)^2 - (\hat{n}_{sub}-1)^2 e^{i\hat{\delta}}}{(\hat{n}_{sub}+1)+(\hat{n}_{sub}-1)e^{i\hat{\delta}}} \left[\frac{\hat{E}_{sub}}{\hat{E}_{film+sub}} - 1 \right], \qquad (10)$$

where the same spectra $\hat{E}_{sub}$ and $\hat{E}_{film+sub}$ as in Tinkham's equation (Eq. 6) are used, or

$$\hat{\sigma}_{film} = \frac{1}{Z_0} \frac{4\hat{n}_{sub}(\hat{E}_{air}/\hat{E}_{film+sub})e^{-2i\pi f d_{sub}(\hat{n}_{sub}-1)/c}}{(\hat{n}_{sub}+1)+(\hat{n}_{sub}-1)e^{i\hat{\delta}}} -$$
$$- \frac{1}{Z_0} \frac{(\hat{n}_{sub}+1)^2 - (\hat{n}_{sub}-1)^2 e^{i\hat{\delta}}}{(\hat{n}_{sub}+1)+(\hat{n}_{sub}-1)e^{i\hat{\delta}}}, \qquad (11)$$

in the case when $\hat{E}_{air}$ and $\hat{E}_{film+sub}$ are used. These equations were obtained for the case of infinite amount of inner reflections. Alternatively, the complex conductance may be extracted from reflection measurements as

$$\hat{\sigma}_{film} = \frac{1}{Z_0} \sqrt{\left(\hat{n}_{sub}+1 - \frac{1}{\hat{r}_{film+sub}+1} \right)^2 - (\hat{n}_{sub}+1)^2 \frac{\hat{r}_{film+sub}-\hat{r}_{sub}}{\hat{r}_{film+sub}+1}} -$$
$$- \frac{1}{Z_0} \left[(\hat{n}_{sub}+1) - \frac{1}{\hat{r}_{film+sub}+1} \right], \qquad (12)$$

where $\hat{r}_{sub}(f)$ is the spectrum of an incident signal reflected from an interface between air and bare substrate, and $\hat{r}_{film+sub}(f)$ is related to signal reflection from an interface between air and substrate covered with a sample film, both divided by reference signal $\hat{r}_{ref}(f)$ of an incident wave reflected from a plane mirror placed instead of a sample. The last equation (Eq. 12) takes into account the presence of an initial pulse and a first inner reflection only. The following discussion involves a validation of the equations for transmitted THz radiation, although the reflection equation presented can be used in the same way.

2.5 Modified Equation Validation by TMM

Using three spectra of a THz wave transmitted through an air $\hat{E}_{air}$, a bare substrate $\hat{E}_{sub}$, and a film-on-substrate effective medium $\hat{E}_{film+sub}$, one may extract an exact substrate complex permittivity dispersion $\hat{\varepsilon}_{sub} = \hat{n}_{sub}^2$ using the Eqs. 1–5 and a film complex permittivity dispersion using the Eq. 10 (or Eqs. 11 or 12) and Eq. 7. According to transfer matrix method [10], these two dispersions may be used to reconstruct an effective complex permittivity dispersion of a film-on-substrate medium and to calculate transmission and reflection coefficients of a THz radiation interacting with this medium.

In the studied case of normal (to the sample plane) incidence of THz radiation onto this two-layer medium, the transfer matrix components are written as

$$
m_{11} = \cos(\hat{k}_{z,film} d_{film}) \cos(\hat{k}_{z,sub} d_{sub})
$$
$$
- \frac{\hat{\eta}_{sub}}{\hat{\eta}_{film}} \sin(\hat{k}_{z,film} d_{film}) \sin(\hat{k}_{z,sub} d_{sub}), \tag{13a}
$$

$$
m_{12} = -\frac{i}{\hat{\eta}_{sub}} \cos(\hat{k}_{z,film} d_{film}) \sin(\hat{k}_{z,sub} d_{sub})
$$
$$
- \frac{i}{\hat{\eta}_{film}} \sin(\hat{k}_{z,film} d_{film}) \cos(\hat{k}_{z,sub} d_{sub}), \tag{13b}
$$

$$
m_{21} = -i\hat{\eta}_{sub} \cos(\hat{k}_{z,film} d_{film}) \sin(\hat{k}_{z,sub} d_{sub})
$$
$$
-i\hat{\eta}_{film} \sin(\hat{k}_{z,film} d_{film}) \cos(\hat{k}_{z,sub} d_{sub}), \tag{13c}
$$

$$
m_{22} = \cos(\hat{k}_{z,film} d_{film}) \cos(\hat{k}_{z,sub} d_{sub})
$$
$$
- \frac{\hat{\eta}_{film}}{\hat{\eta}_{sub}} \sin(\hat{k}_{z,film} d_{film}) \sin(\hat{k}_{z,sub} d_{sub}), \tag{13d}
$$

where $k_0 = 2\pi f/c$ is the free-space wave number, $\hat{k}_{z,film} = k_0 \sqrt{\hat{\varepsilon}_{film}}$, $\hat{k}_{z,sub} = k_0 \sqrt{\hat{\varepsilon}_{sub}}$, $\hat{\eta}_{film} = 2\pi f \varepsilon_0 \hat{\varepsilon}_{film}/\hat{k}_{z,film}$, and $\hat{\eta}_{sub} = 2\pi f \varepsilon_0 \hat{\varepsilon}_{sub}/\hat{k}_{z,sub}$. Using these components, one may extract the magnitude transmission spectrum of a film-on-substrate effective structure as

$$
|\hat{t}| = |\frac{2\eta_0}{m_{11}\eta_0 + m_{12}\eta_0^2 + m_{21} + m_{22}\eta_0}|, \tag{14}
$$

where $\eta_0 = 1/Z_0$.

Comparing a magnitude transmission coefficient $|\hat{t}|$ calculated using TMM with that measured in an experiment ($|\hat{E}_{film+sub}|/|\hat{E}_{air}|$) allows one to estimate accuracy of the Eqs. 10–12 derived in this work.

2.6 Fitting of a Complex Conductivity Dispersion by Drude or Drude-Smith Model

Extracted complex conductivity dispersion of a thin film may be compared with theoretical predictions provided for electron gas in conductive materials. The Drude-Smith model is a modification of the classical Drude conductivity model which takes into account a localization of carriers [11]:

$$
\hat{\sigma}_{film} = \frac{W}{1 - 2i\pi f\tau} \left(1 + \frac{C}{1 - 2i\pi f\tau}\right), \tag{15}
$$

where W is a Drude weight, $\sigma_0 = W(1+C)$ is a DC conductivity, τ is a carrier relaxation time, and C is the so-called backscattering parameter denoting the localization of carriers which can vary from 0 (free carriers) to -1 (completely localized carriers).

When $C = 0$, this equation is simplified to the classical Drude model. As a result, extracted parameter values may be compared with those given in other works.

3 Results and Discussion

Typical examples of thin-film conductive materials used in the THz frequency range, namely bismuth and graphene, were chosen to study in this work. For example, an accurate dispersion of a thin film complex conductivity may be applied in modeling of a THz radiation detector based on such a material [21, 22]. Bismuth film with the thickness of 120 nm was sprayed onto 21 μm mica dielectric substrate by thermal evaporation in vacuum [23, 24]; single-layer graphene with an atomic thickness esti- mated to be about 0.345 nm [25] was grown using chemical vapor deposition and then was placed on the top of 53 μm thick PET (polyethylene terephthalate) substrate [26]. The results of THz TDS experiment and data processing are presented in Figs. 2, 3, 4, 5, 6, and 7.

The waveforms of THz radiation measured by THz TDS are presented in Fig. 2. The left graph corresponds to structure consisting of Bi film on mica substrate, and the right graph corresponds to graphene single layer on PET substrate. The length of waveforms defines the frequency resolution of these measurements: this length is equal to 276 ps (frequency resolution of 3.62 GHz, temporal resolution of 0.0833 ps, 3313 time points) for Bi/mica and to 40 ps (frequency resolution of 25 GHz, temporal resolution of 0.0469 ps, 855 time points) for graphene/PET. The temporal constant is 100 ms. An increase in length of these waveforms makes it possible to obtain necessary frequency resolution of the dispersions, but does not change their shape and position in general.

Then, the amplitude and phase spectra are extracted by fast Fourier transform (FFT) method (Fig. 3). The frequency range of measurements is equal to 0.2−1.0 THz as the power of THz radiation generator is distributed mainly in this range allowing for
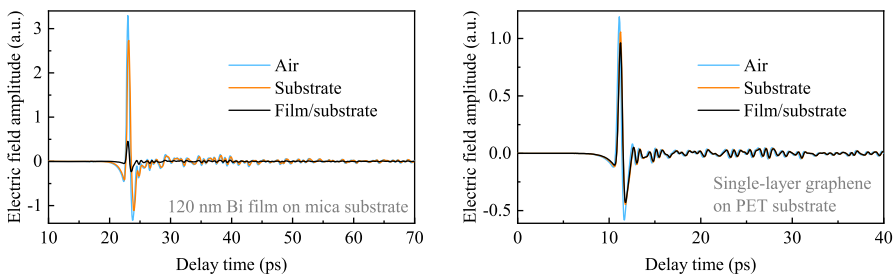

Fig. 2 Waveforms of THz pulses passed through the air, the bare substrates, and the film-on-substrate structures for the cases of Bi/mica (left graph) and graphene/PET (right graph)
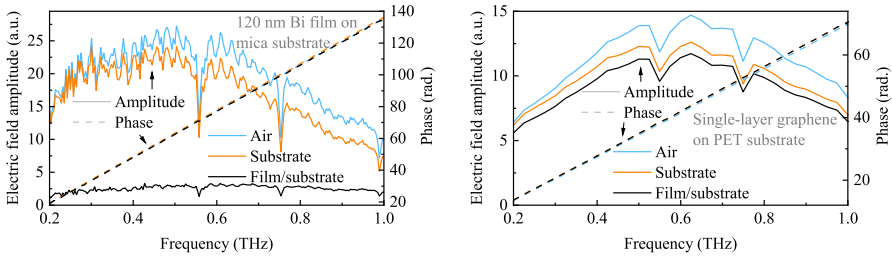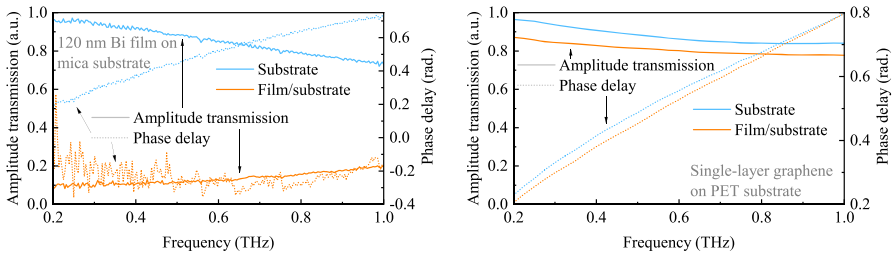
Fig. 3 Amplitude and phase spectra of THz pulses passed through the air, the bare substrates, and the film-on-substrate structures for the cases of Bi/mica (left graph) and graphene/PET (right graph)

Fig. 4 Amplitude transmission and phase delay spectra of bare substrates and the film-on-substrate structures for the cases of Bi/mica (left graph) and graphene/PET (right graph), normalized as $|\hat{E}_{sub}(f)|/|\hat{E}_{air}(f)|$, $|\hat{E}_{film+sub}(f)|/|\hat{E}_{air}(f)|$ and $\phi_{sub}(f) - \phi_{air}(f)$, $\phi_{film+sub}(f) - \phi_{air}(f)$
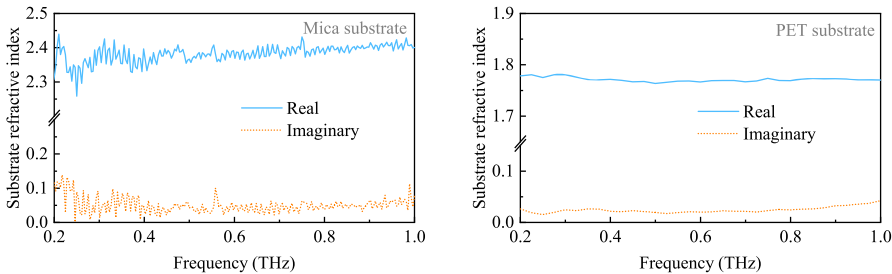

Fig. 5 Dispersions of real and imaginary parts of the refractive index for the cases of mica (left graph) and PET (right graph) substrates
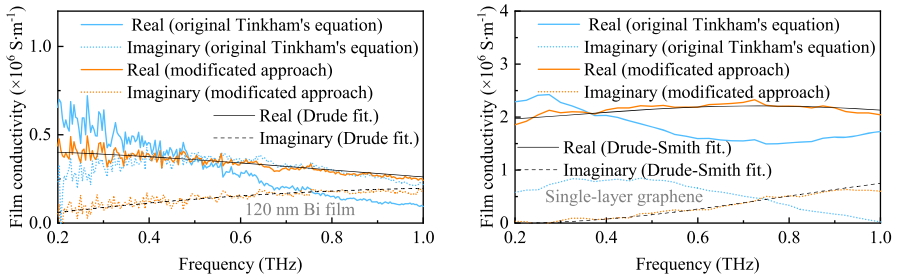
Fig. 6 Dispersions of real (solid curves) and imaginary (dot curves) parts of complex conductivity for the cases of 120 nm bismuth film (left graph) and single-layer graphene (right graph) calculated using original Tinkham's equation (blue curves) and modified equation (orange curves). The black curves correspond to fitting by the Drude-Smith model

a high dynamic range of measurements. The amplitude transmission and phase delay spectra are shown in Fig. 4 as they are used in further calculations.

Figure 5 depicts the dispersions of complex refractive index of 21 μm mica and 53 μm PET substrates which are calculated using the iterative method discussed above (see Eqs. 1-5).

The refractive index dispersions of mica and PET substrates are substituted into original Tinkham's equation (Eq. 6) and into modified equation derived in this work (Eq. 10). The resulting complex sheet conductivity dispersions of 120 nm Bi and single-layer graphene are presented in Fig. 6. They may be fitted with the classical Drude model or with the Drude-Smith model (see Eq. 15). The following parameter values are obtained for 120 nm Bi film: DC conductivity $\sigma_0 = 0.41 \cdot 10^6$ S·m^{-1}, carrier relaxation time $\tau = 123$ fs, and localization $C = 0$ matching the classical Drude model. These parameters are well-consistent with previous results [27, 28]. For graphene single-layer, the parameters are equal to $\sigma_0 = 1.91 \cdot 10^6$ S·m^{-1}, $\tau = 130$ fs, and $C = -0.52$ highlighting the presence of scattering impurities in graphene. These parameters are very close to those for few-layer graphene [29]. Thus, 120 nm Bi film
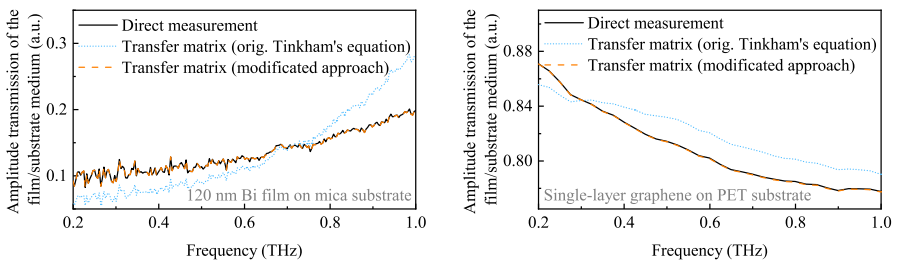

Fig. 7 Amplitude transmission spectra of the film-on-substrate Bi/mica (left graph) and graphene/PET (right graph) structures measured in the experiment (black solid curves) and calculated by TMM using conductive films permittivity dispersion obtained by original Tinkham's method (blue dotted curves) and by modified approach (orange dashed curves)

is a solid (continuous) film, and the electrons in single-layer graphene are affected by backward scattering as a result of the structural disorder effects [30]. The fitting curves are also presented in Fig. 6. These curves agree well with the conductivity dispersions calculated from the modified equation.

To estimate accuracy of the approach derived in this work, TMM was used. The complex sheet conductivity dispersions presented above were converted into complex permittivity dispersions using Eq. 7. Then, they were substituted into Eq. 13 to calculate an amplitude transmission spectrum of a film-on-substrate medium by Eq. 14. The results of calculation are shown in Fig. 7 along with amplitude transmission spectra measured in the experiment ($|\hat{E}_{film+sub}|/|\hat{E}_{air}|$). As it can be seen, the modified approach of a film THz conductivity extraction is fully confirmed by the calculation based on TMM. It should be mentioned that there is a work considering the same case of a thin conductive film on a dielectric substrate [31], but the equation derived in the mentioned work differs by several terms from the equation derived in our work, and its substitution into TMM does not fit the amplitude transmission measured directly.

4 Conclusion

The accurate approach to extraction of an exact complex THz conductivity of an ultra-thin conductive film on a dielectric substrate was derived in this work. This method does not require filtering experimental data of terahertz time-domain spectroscopy (THz waveforms) and thus does not distort the information on material parameters of a sample. It may be used even for very thin films and lossy substrates with internal reflections close to each other on a THz waveform when they are difficult to filter. It should be mentioned that this work is devoted to the improvement of material parameters extraction accuracy, while instrumental errors depend on experimental details, such as alignment, dynamic range, and micrometer accuracy. The approach was tested on 120 nm Bi film on mica substrate and on graphene monolayer placed on PET substrate. In conclusion, the accuracy of the presented method was confirmed by calculations based on the transfer matrix method and by dispersion fitting using the Drude-Smith model. Exact THz complex conductivity dispersions of various thin films extracted using the derived equations may be applied in the numerical simulation of various THz components, such as emitters and detectors, devices modulating amplitude, phase and polarization of THz radiation for wireless communication systems, visualization in medicine and security systems, and non-contact control of food, drugs.

Author Contributions M.K.K. supervised the investigation; A.D.Z. and M.S.M. wrote the manuscript. P.S.D. performed the majority of the measurements. All authors contributed to the study conception and methodology, data collection, and analysis. All authors read and approved the manuscript.

Code Availability Not applicable

Declarations

Ethics Approval Not applicable

Consent to Participate Not applicable

Consent for Publication Not applicable

Conflict of Interest The authors declare no competing interests.

References

1. Mukherjee, P., Gupta, B.: Terahertz (THz) frequency sources and antennas – a brief review. International Journal of Infrared and Millimeter Waves 29(12), 1091–1102 (2008)
2. Sizov, F.: Terahertz radiation detectors: the state-of-the-art. Semiconductor Science and Technology 33(12), 123001 (2018)
3. Ummy, M., Hossain, A., Bikorimana, S., Dorsinville, R.: A dual-wavelength widely tunable C-band SOA-based fiber laser for continuous wave terahertz generation. In: Optics, Photonics and Laser Technology 2018, pp. 119–141. Springer, Cham, Switzerland (2019)
4. Mathanker, S.K., Weckler, P.R., Wang, N.: Terahertz (THz) applications in food and agriculture: A review. Transactions of the ASABE 56(3), 1213–1226 (2013)
5. Corsi, C., Sizov, F. (eds.): THz and Security Applications: Detectors, Sources and Associated Electronics for THz Applications. Springer, Dordrecht, Netherlands (2014)
6. Kürner, T., Priebe, S.: Towards THz communications – status in research, standardization and regulation. Journal of Infrared, Millimeter, and Terahertz Waves 35(1), 53–62 (2014)
7. Laman, N., Grischkowsky, D.: Terahertz conductivity of thin metal films. Applied Physics Letters 93(5), 051105 (2008)
8. Yan, S., Li, Z., Wei, D., Cui, H.-L., Du, C.: Sheet conductance and imaging of graphene by terahertz time-domain spectroscopy. In: 2016 IEEE International Conference on Manipulation, Manufacturing and Measurement on the Nanoscale (3M-NANO), pp. 339–342 (2016). IEEE
9. Tinkham, M.: Energy gap interpretation of experiments on infrared transmission through superconducting films. Physical Review 104(3), 845 (1956)
10. Qi, L., Liu, C.: Complex band structures of 1D anisotropic graphene photonic crystal. Photonics Research 5(6), 543–551 (2017)
11. Shimakawa, K., Itoh, T., Naito, H., Kasap, S.: The origin of non-Drude terahertz conductivity in nanomaterials. Applied Physics Letters 100(13), 132102 (2012)
12. Song, Q., Chen, H., Zhang, M., Li, L., Yang, J., Yan, P.: Broadband electrically controlled bismuth nanofilm THz modulator. APL Photonics 6(5), 056103 (2021)
13. Wang, M., Yang, E.-H.: THz applications of 2D materials: Graphene and beyond. Nano-Structures & Nano-Objects 15, 107–113 (2018)
14. Liu, J., Lyu, W., Deng, X., Wang, Y., Geng, H., Zheng, X.: Material and thickness selection of dielectrics for high transmittance terahertz window and metasurface. Optical Materials 127, 112219 (2022)
15. Naftaly, M., Miles, R.E.: Terahertz time-domain spectroscopy for material characterization. Proceedings of the IEEE 95(8), 1658–1665 (2007)
16. Naftaly, M. (ed.): Terahertz Metrology. Artech House, Norwood, MA, USA (2015)
17. Taschin, A., Bartolini, P., Tasseva, J., Torre, R.: THz time-domain spectroscopic investigations of thin films. Measurement 118, 282–288 (2018)
18. Novotny, L., Hecht, B.: Principles of Nano-optics. Cambridge university press, Cambridge, UK (2012)
19. Tomaino, J., Jameson, A., Kevek, J., Paul, M., Van Der Zande, A., Barton, R., McEuen, P., Minot, E., Lee, Y.-S.: Terahertz imaging and spectroscopy of large-area single-layer graphene. Optics express 19(1), 141–146 (2011)
20. Arcos, D., Gabriel, D., Dumcenco, D., Kis, A., Ferrer-Anglada, N.: THz time-domain spectroscopy and IR spectroscopy on MoS_2. Physica Status Solidi (b) 253(12), 2499–2504 (2016)

21. Khodzitsky, M., Tukmakova, A., Zykov, D., Novoselov, M., Tkhorzhevskiy, I., Sedinin, A., Novotelnova, A., Zaitsev, A., Demchenko, P., Makarova, E., et al.: THz room-temperature detector based on thermoelectric frequency-selective surface fabricated from $Bi_{88}Sb_{12}$ thin film. Applied Physics Letters 119(16), 164101 (2021)

22. Tukmakova, A., Tkhorzhevskiy, I., Sedinin, A., Asach, A., Novotelnova, A., Kablukova, N., Demchenko, P., Zaitsev, A., Zykov, D., Khodzitsky, M.: FEM simulation of frequency-selective surface based on thermoelectric Bi-Sb thin films for THz detection. Photonics 8(4), 119 (2021)

23. Grabov, V., Demidov, E., Komarov, V.: Optimization of the conditions for vacuum thermal deposition of bismuth films with control of their imperfection by atomic force microscopy. Physics of the Solid State 52(6), 1298–1302 (2010)

24. Zaitsev, A., Zykov, D., Demchenko, P., Novoselov, M., Nazarov, R., Masyukov, M., Makarova, E., Tukmakova, A., Asach, A., Novotelnova, A., et al.: Experimental investigation of optically controlled topological transition in bismuth-mica structure. Scientific Reports 11(1), 1–13 (2021)

25. De Lima, L.R.M., Martins, F.P., Lagarinhos, J.N., Santos, L., Lima, P., Torcato, R., Marques, P.A., Rodrigues, D.L., Melo, S., Grilo, J., et al.: Characterization of commercial graphene-based materials for application in thermoplastic nanocomposites. Materials Today: Proceedings 20, 383–390 (2020)

26. Zaitsev, A., Grebenchukov, A., Demchenko, P., Alonso, E., Craciun, M., Russo, S., Baldycheva, A., Khodzitsky, M.: The study of optical properties of graphene intercalated with ferric chloride for application in terahertz photonics. In: Journal of Physics: Conference Series, vol. 1124, p. 071007 (2018). IOP Publishing

27. Katayama, I., Minami, Y., Arashida, Y., Handegard, O.S., Nagao, T., Kitajima, M., Takeda, J.: Nonlinear terahertz dynamics of Dirac electrons in Bi thin films. In: Terahertz Emitters, Receivers, and Applications IX, vol. 10756, pp. 64–70 (2018)

28. Cho, S., DiVenere, A., Wong, G.K., Ketterson, J.B., Meyer, J.R.: Transport properties of $Bi_{1-x}Sb_x$ alloy thin films grown on CdTe (111) B. Physical Review B 59(16), 10691 (1999)

29. Grebenchukov, A.N., Zaitsev, A.D., Novoselov, M.G., Demchenko, P.S., Kovalska, E.O., Alonso, E.T., Walsh, K., Russo, S., Craciun, M.F., Baldycheva, A.V., et al.: Photoexcited terahertz conductivity in multi-layered and intercalated graphene. Optics Communications 459, 124982 (2020)

30. Dadrasnia, E., Lamela, H., Kuppam, M., Garet, F., Coutaz, J.-L.: Determination of the DC electrical conductivity of multiwalled carbon nanotube films and graphene layers from noncontact time-domain terahertz measurements. Advances in Condensed Matter Physics 2014 (2014)

31. Whelan, P.R., Huang, D., Mackenzie, D., Messina, S.A., Li, Z., Li, X., Li, Y., Booth, T.J., Jepsen, P.U., Shi, H., et al.: Conductivity mapping of graphene on polymeric films by terahertz time-domain spectroscopy. Optics express 26(14), 17748–17754 (2018)